Low-complexity Delay-Doppler Symbol DNN for OTFS Signal Detection

Ashwitha Naikoti and A. Chockalingam
Department of ECE, Indian Institute of Science, Bangalore 560012

***Abstract*—In this paper, we consider the problem of low-complexity detection of orthogonal time frequency space (OTFS) modulation signals using deep neural networks (DNN). We consider a DNN architecture in which each symbol multiplexed in the delay-Doppler grid is associated with a separate DNN. The considered symbol-level DNN has fewer parameters to learn compared to a full DNN that takes into account all symbols in an OTFS frame jointly, and therefore has less complexity. Under the assumption of static multipath channel with i.i.d. Gaussian noise, our simulation results show that the performance of the symbol-DNN detection is quite close to that of the full-DNN detection as well as the maximum-likelihood (ML) detection. Further, when the noise model deviates from the standard i.i.d. Gaussian model (e.g., non-Gaussian noise with t-distribution), because of its ability to learn the distribution, the symbol-DNN detection is found to perform better than the ML detection. A similar performance advantage is observed in multiple-input multiple-output OTFS (MIMO-OTFS) where the noise across multiple received antennas are correlated.**

Keywords *– OTFS modulation, delay-Doppler domain, deep neural networks, signal detection, non-standard channels.*

I. Introduction

Orthogonal time frequency space (OTFS) modulation [1] is an emerging modulation technique that performs superior compared to the currently prevalent orthogonal frequency division multiplexing (OFDM) in high-Doppler environments [2], [3]. It is a two-dimensional modulation technique in which the information symbols are multiplexed in the delay-Doppler (DD) domain instead of the time-frequency domain [4]- [6]. OTFS can be implemented on top of popular multicarrier modulation schemes (such as OFDM) by adding extra pre-processing and post-processing blocks [7]. Further to the superior performance of OTFS compared to OFDM in high-mobility scenarios (e.g., 500 km/h in 4 GHz band [2]), it has been shown that OTFS outperforms OFDM in static multipath channels as well [8]. The reason behind this better performance has been identified to be the structural equivalence between OTFS and asymmetric OFDM (A-OFDM) in [9]. This observation allows OTFS to be considered for use in a wide range of no- to high-mobility scenarios. Our current focus in this paper is the exploration of the use of deep neural networks (DNN) for the detection of OTFS signals. Motivated by the better performance of OTFS in static multipath channels, we initially consider the use of DNNs in OTFS signal detection in static multipath channels. We also observe that the DNN approach can do well in non-zero Doppler scenarios as well, due to the long channel coherence in the delay-Doppler domain. Another key highlight of the considered DNN approach is the low-complexity aspect, which is achieved through modularizing the DNN architecture at the delay-Doppler symbol level.

DNNs have found popular use in various fields. Their use in the physical layer design in wireless communications is getting increased research attention [10]. Constellation design, transceiver design, codes design using autoencoders, signal detection and demodulation are some of the areas where DNNs have been successfully employed [11]- [18]. Here, we focus on the detection of OTFS signals. One approach to do detection of multi-dimensional signals is to use a single fully connected DNN where the number of input neurons is decided by the size of the received/observed vector and the number of output neurons is decided by the size of the multi-dimensional signal set. Hence, each neuron in the output layer corresponds to one transmit signal vector from the signal set, enabling joint detection of the multi-dimensional symbol vector. While this approach is architecturally simple and straightforward, it requires a large number of parameters to be learned. This is because the number of output neurons grows exponentially in the size of transmit symbol vector, requiring a proportionately large number of neurons in the hidden layers. An alternate approach is to devise multiple DNNs, one for each symbol in the transmit symbol vector. This approach has the benefit of low complexity because the number of DNNs grows linearly with the size of the transmit symbol vector and the number of output neurons in each DNN also grows linearly in the size of the symbol alphabet [16]. We consider the latter approach in this paper for OTFS detection where the transmit vector consists of symbols multiplexed in the delay-Doppler domain.

Our results show that, under the assumption of static multipath channel with i.i.d. Gaussian noise, the performance of the 'symbol-DNN' detection is close to that of the 'full-DNN' detection as well as the maximum-likelihood (ML) detection. Owing to the long channel coherence in the DD domain, the DNN approach is also found to work well in non-zero Doppler cases as well. Additional benefits of using DNN for OTFS detection show up when the noise model deviates from the standard i.i.d. Gaussian model. We consider deviations from the Gaussian as well as independence assumptions. For deviation from the Gaussian assumption, we consider t-distribution (which is close to Gaussian distribution) for noise. For deviation from the independence assumption, we consider spatially correlated noise across receive antennas in a MIMO-OTFS system. In both the cases of deviations, because of the ability of the DNN to learn the underlying noise distribution, the symbol-DNN detection outperforms ML detection, which is optimum only for the standard i.i.d. Gaussian noise model.

This work was supported in part by the J. C. Bose National Fellowship, Department of Science and Technology, Government of India.

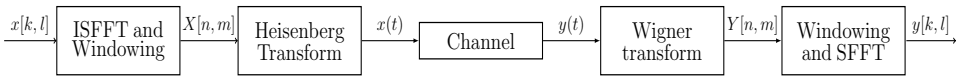

Fig. 1. OTFS modulation scheme.

The rest of the paper is organized as follows. The considered OTFS system model is presented in Sec. II. The symbol-DNN for OTFS signal detection is presented in Sec. III. Simulation results and discussions are presented in Sec. IV. Conclusions are presented in Sec. V.

II. OTFS System Model

In this section, we present the OTFS system model and the vectorized formulation of the input-output relation. Figure 1 shows the OTFS modulation scheme.

The OTFS transmitter uses an $N\times M$ delay-Doppler grid for multiplexing information symbols. There are NM information symbols, each from a modulation alphabet $\mathbb{A}$, denoted by $x[k,l]$, $k=0,\cdots,N-1$, $l=0,\cdots,M-1$. These NM symbols are transmitted in a duration of NT, occupying a bandwidth of $M\Delta f$, where $\Delta f=1/T$. The symbols in the two-dimensional $N\times M$ delay-Doppler grid are transformed to the time-frequency (TF) plane using inverse symplectic finite Fourier transform (ISFFT), as

$$X[n,m]=\frac{1}{MN}\sum_{k=0}^{N-1}\sum_{l=0}^{M-1}x[k,l]e^{j2\pi(\frac{nk}{N}-\frac{ml}{M})}. \quad (1)$$

Heisenberg transform is then applied such that the TF signal is converted into a time domain signal $x(t)$ for transmission through the wireless channel, as

$$x(t)=\sum_{n=0}^{N-1}\sum_{m=0}^{M-1}X[n,m]g_{tx}(t-nT)e^{j2\pi m\Delta f(t-nT)}, \quad (2)$$

where $g_{tx}(t)$ is the transmit pulse shape. With τ and ν denoting the delay and the Doppler variables, respectively, the received time domain signal $y(t)$ at the receiver is given by

$$y(t)=\int_\nu\int_\tau h(\tau,\nu)x(t-\tau)e^{j2\pi\nu(t-\tau)}d\tau d\nu, \quad (3)$$

where $h(\tau,\nu)$ is the delay-Doppler domain baseband response of the channel.

The received signal $y(t)$ is transformed using Wigner transform into a TF signal, as

$$Y[n,m]=A_{g_{rx},y}(t,f)|_{t=nT,f=m\Delta f}, \quad (4)$$

$$A_{g_{rx},y}(t,f)=\int g^*_{rx}(t'-t)y(t)e^{-j2\pi f(t'-t)}dt',$$

where $g_{rx}(t)$ is the receive pulse shape. If $g_{rx}(t)$ and $g_{tx}(t)$ satisfy the condition of biorthogonality [2], the following equation gives the input-output relation in the TF domain:

$$Y[n,m]=H[n,m]X[n,m]+V[n,m], \quad (5)$$

where $V[n,m]$ is the additive white Gaussian noise after Wigner transformation and $H[n,m]$ is given by

$$H[n,m]=\int_\tau\int_\nu h(\tau,\nu)e^{j2\pi\nu nT}e^{-j2\pi(\nu+m\Delta f)\tau}d\nu d\tau. \quad (6)$$

The TF signal $Y[n,m]$ in (5) is mapped to the delay-Doppler domain signal $y[k,l]$ by applying symplectic finite Fourier transform (SFFT), as

$$y[k,l]=\sum_{n=0}^{N-1}\sum_{m=0}^{M-1}Y[n,m]e^{-j2\pi(\frac{nk}{N}-\frac{ml}{M})}. \quad (7)$$

The input-output relation can be written in the form [2]

$$y[k,l]=\frac{1}{MN}\sum_{l'=0}^{N-1}\sum_{k'=0}^{M-1}x[k',l']h_w(\frac{k-k'}{NT},\frac{l-l'}{M\Delta f})+v[k,l], \quad (8)$$

where $h_w(\nu,\tau)$ is the circular convolution of the channel response with a windowing function $w(\nu,\tau)$ and $h_w(\frac{k-k'}{NT},\frac{l-l'}{M\Delta f})=h_w(\nu,\tau)|_{\nu=\frac{k-k'}{NT},\tau=\frac{l-l'}{M\Delta f}}$.

Now, consider a DD channel with P paths which can be represented as

$$h(\tau,\nu)=\sum_{i=1}^{P}h_i\delta(\tau-\tau_i)\delta(\nu-\nu_i), \quad (9)$$

where h_i,τ_i, and ν_i are the channel gain, delay, and Doppler shift corresponding to the ith path, respectively. We assume $\tau_i\triangleq\frac{\alpha_i}{M\Delta f}$ and $\nu_i\triangleq\frac{\beta_i}{NT}$ where α_i,β_i are integers. Assuming that the receive and the transmit window functions $W_{rx}[n,m]$ and $W_{tx}[n,m]$ are rectangle, the input-output relation for the channel in (9) is as follows [5]:

$$y[k,l]=\sum_{i=1}^{P}h'_ix[(k-\beta_i)_N,(l-\alpha_i)_M]+v[k,l]. \quad (10)$$

In (10), we have h'_is as $h'_i=h_ie^{-j2\pi\nu_i\tau_i}$. Here, h_is are i.i.d. $\mathcal{CN}(0,1/P)$ distributed. The input-output relationship can thus be represented in a vectorized form as [5]

$$\mathbf{y}=\mathbf{H}\mathbf{x}+\mathbf{v}, \quad (11)$$

where $\mathbf{x},\mathbf{y},\mathbf{v}\in\mathbb{C}^{MN\times1}$ and $\mathbf{H}\in\mathbb{C}^{MN\times MN}$. The $x[k,l]$ element in the delay-Doppler grid is the $(k+Nl)$th element in $\mathbf{x}$, $k=0,\cdots,N-1, l=0,\cdots,M-1$, and $x[k,l]\in\mathbb{A}$. This vectorized representation is used as the system model for detection. Assuming that the channel matrix $\mathbf{H}$ is known at the receiver, the decision rule for maximum likelihood detection of OTFS signal is given by

$$\hat{\mathbf{x}}=\underset{\mathbf{x}\in\mathbb{A}^{MN}}{\arg\min}\ \|\mathbf{y}-\mathbf{H}\mathbf{x}\|^2. \quad (12)$$

It is noted that (12) is the optimal detection rule only when the noise distribution is i.i.d. Gaussian, and it will result in sub-optimal detection when the noise model deviates from the standard i.i.d. Gaussian model.

III. Symbol-DNN for OTFS detection

OTFS signal detection involves the detection of the MN symbols multiplexed in the DD grid, i.e., we need to estimate the $MN \times 1$ transmitted vector $\mathbf{x}$ given the knowledge of received vector $\mathbf{y}$ and the DD channel matrix $\mathbf{H}$. In this section, we present the DD symbol-DNN for OTFS detection.

The DD symbol-DNN architecture for OTFS detection is shown in Fig. 2. It consists of MN DD symbol-DNNs, each corresponding to an individual information symbol in the DD grid. There are $2MN$ input neurons in all these symbol-DNNs through which the real and the imaginary parts of the received vector $\mathbf{y}$ are given as input to the network. The number of output neurons in each of the DNNs is equal to $|\mathbb{A}|$, the size of the modulation alphabet, such that each output neuron gives the corresponding probability of each symbol in the alphabet being transmitted. Softmax activation is used in the output layer such that all the probabilities of the symbols in the alphabet are dependent and sum to one. The symbol mapper chooses the symbol corresponding to the highest probability as the transmitted symbol.

A. Training and testing

The channel models considered are *i*) static multipath channel with zero Doppler and *ii*) multipath channel with non-zero Doppler. In the non-zero Doppler case also, the DD channel variations are slow because rapid channel variations in the time domain become slow variations when viewed in the DD domain. This is a key advantage of the DD signaling in OTFS which allows effective training of the DNNs. The DNNs can be trained by a set of training examples $\mathbf{x}_T$ known both at the transmitter and the receiver. The training examples are pseudo-randomly generated by the transmitter and are sent to the receiver through the channel. The received signal vector $\mathbf{y}$ generated according to the system model in (11) and the transmitted signal vector $\mathbf{x}_T$ are available to the receiver. The real and imaginary parts of $\mathbf{y}$ are given as input to the symbol-DNNs. The number of training examples to be used for training is chosen by trial. Initially, we start with a small number of examples and increment it until the performance of the trained DNN is good. Once trained, the DNNs can be used for signal detection (testing phase). During the testing phase, the transmitter randomly generates information bits, modulates them using OTFS and transmits them through the channel. The receiver detects each symbol in the DD frame by using the already trained symbol-DNNs. Each symbol-DNN learns the mapping from the received vector to the corresponding symbol in the transmitted vector. As the channel is static/slowly varying, the DNNs as a whole are performing the task of a channel equalizer and hence the channel need not be explicitly known at the receiver during training. Training and testing are carried out using Tensorflow and Keras framework.

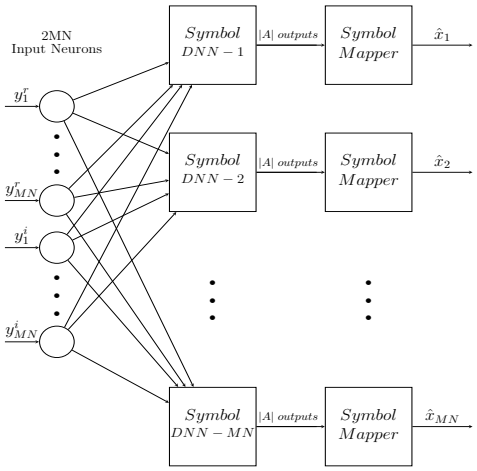

Fig. 2. Delay-Doppler symbol-DNN architecture.

IV. Simulation results

In this section, we present the simulated bit error rate (BER) performance of the symbol-DNN based OTFS detection. We also compare its performance with those of full-DNN detection, ML detection, and MMSE detection. We also present a complexity comparison among these detectors.

A. BER in static multipath channel with i.i.d. Gaussian noise

Figure 3 shows the BER performance of OTFS using symbol-DNN detection, full-DNN detection, and ML detection in a system with $M = N = 4$ and BPSK. A carrier frequency (f_c) of 4 GHz and a subcarrier spacing (Δf) of 3.75 KHz are considered. A static (zero Doppler) multipath channel with $P = 2$ paths with uniform power profile on the delay axis is considered. The noise is assumed to be i.i.d. Gaussian. For $M = N = 2$ and BPSK, there are $MN = 4$ BPSK information symbols in a frame. The symbol-DNN architecture has four DNNs, one for each BPSK symbol in the transmit symbol vector. The parameters used in the symbol-DNN as well as the full-DNN are listed in Table I. The architectures used for symbol-DNN and full-DNN are as follows:
i) Symbol-DNN: input $\rightarrow$ 8 $\rightarrow$ ReLU $\rightarrow$ 4 $\rightarrow$ ReLU $\rightarrow$ 2 $\rightarrow$ Softmax.
ii) Full-DNN: input $\rightarrow$ 8 $\rightarrow$ ReLU $\rightarrow$ 12 $\rightarrow$ ReLU $\rightarrow$ 16 $\rightarrow$ Softmax.
The numbers mentioned above are the number of neurons in a given layer and are followed by the activation function used in that layer. For Full-DNN detector, onehot encoding is used.

From Fig. 3, it can be seen that the BER performance of OTFS using both the symbol-DNN as well as the full-DNN detection are almost the same as the performance of ML detection. This demonstrates the good detection performance achieved by the DNN approach. Although all the three detectors achieve very close performance, their complexities are different. Table II shows the complexities of the three detectors in number of real operations. It can be seen that ML detection has the highest complexity because of the exhaustive enumeration of all possible OTFS transmit vectors. Among the DNNs, symbol-DNN has a lower complexity compared to

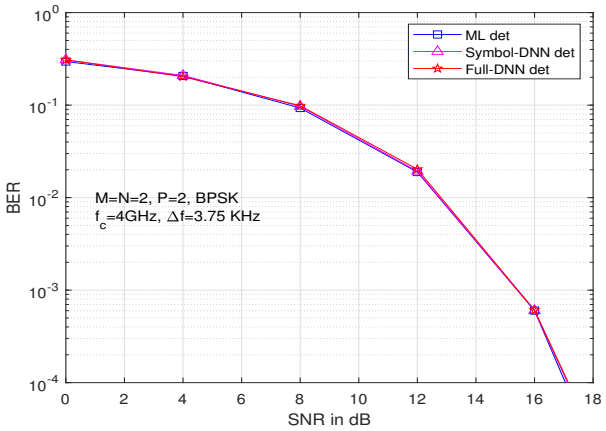

Fig. 3. BER performance of OTFS with $M = N = 2$ using symbol-DNN, full-DNN and ML detection in static multipath channel with $P = 2$.

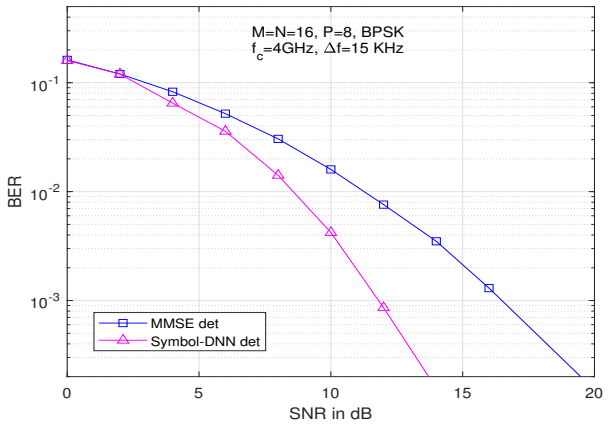

Fig. 4. BER performance of OTFS with $M = N = 16$ using symbol-DNN and MMSE detection in static multipath channel with $P = 8$.

Parameters	Symbol-DNN	Full-DNN
No. of input neurons	$2MN = 8$	$2MN = 8$
No. of output neurons	$\|\mathbb{A}\| = 2$	$2^{MN} = 16$
No. of hidden layers	1	1
Hidden layer activation	ReLU	ReLU
Output layer activation	Softmax	Softmax
Optimization	Adam	Adam
Loss function	Binary crossentropy	Categorical crossentropy
Training SNR	10 dB	10 dB
No. of training examples	30,000	30,000
No. of epochs	50	50

TABLE I
PARAMETERS OF DNN DETECTORS IN FIG. 3.

full-DNN. This is because the number of parameters to train in full-DNN is larger than in symbol-DNN, as can be observed in Table II.

Detector	ML det.	Symbol-DNN det.	Full-DNN det.
Complexity	1088	304	564
Trainable parameters	-	184	316

TABLE II
COMPLEXITY (IN NO. OF REAL OPERATIONS) OF DETECTORS IN FIG. 3.

We next consider the performance of a larger OTFS system with a larger DD grid. Towards this, we consider a system with $M = N = 16$ (i.e., $MN = 256$ symbols per frame), BPSK, $f_c = 4$ GHz, $\Delta f = 15$ KHz, and $P = 8$. Here, we consider symbol-DNN detection and minimum mean square error (MMSE) detection due to their low complexities. ML detection for this system must do exhaustive search over 2^{256} signal vectors, which becomes computationally infeasible. Full-DNN detection for this large system will have $2^{MN} = 2^{256}$ output neurons, and hence the size of the full-DNN will be large with many trainable parameters. The symbol-DNN architecture used for detection in this system is as follows.

Symbol-DNN: input $\rightarrow$ 512 $\rightarrow$ ReLU $\rightarrow$ 256 $\rightarrow$ ReLU $\rightarrow$ 2 $\rightarrow$ Softmax.

There are $MN = 256$ such symbol-DNNs that constitute the detector. Each symbol-DNN is trained using the parameters in Table III. Figure 4 shows the BER performance using symbol-DNN detection and MMSE detection. It can be seen that symbol-DNN detection achieves significantly better performance compared to MMSE detection. For example, symbol-DNN performs better by about 4 dB at 10^{-3} BER. Table IV shows the complexities of the two detectors in number of real operations. It is observed that the symbol-DNN detector performs better than the MMSE detection and is computationally efficient.

Parameters	Symbol-DNN
No. of input neurons	$2MN$ = 512
No. of output neurons	$\|\mathbb{A}\| = 2$
No. of hidden layers	1
Hidden layer activation	ReLU
Output layer activation	Softmax
Optimization	Adam
Loss function	Binary crossentropy
Training SNR	8 dB
No. of training examples	80,000
No. of epochs	20

TABLE III
PARAMETERS OF SYMBOL-DNN DETECTOR IN FIG. 4.

Detector	Complexity	Trainable parameters
MMSE det	83951616	-
Symbol DNN det	67305472	33751552

TABLE IV
COMPLEXITY (IN NO. OF REAL OPERATIONS) OF DETECTORS IN FIG. 4.

B. BER in static multipath channel with non-Gaussian noise

Here, we consider the scenario in which the multipath channel is static with zero Doppler but the noise is non-Gaussian. As an example, we consider the case when the noise follows t-distribution with parameter μ. This distribution gets closer to Gaussian for larger values of μ. Figure 6 shows the performance of symbol-DNN and ML detectors when the noise is t-distributed with parameter $\mu = 5$. The performance of ML detection with i.i.d. Gaussian noise is also plotted for comparison. The system parameters considered are: $f_c = 4$ GHz, $\Delta f = 3.75$ kHz, $M = N = 2$, $P = 2$, and BPSK. The

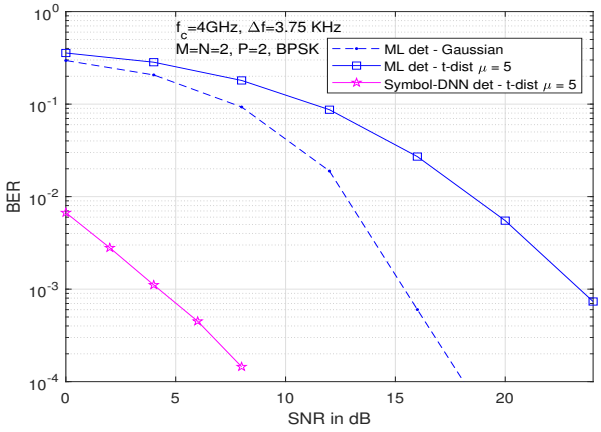

Fig. 5. BER performance of OTFS with $M = N = 2$ in static channel with $P = 2$ using symbol-DNN and ML detectors under t-distributed noise.

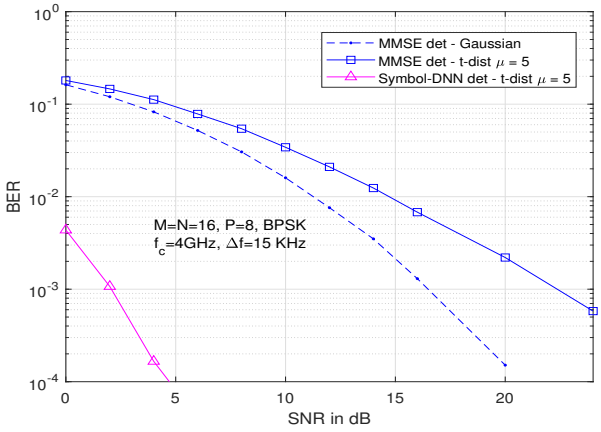

Fig. 6. BER performance of OTFS with $M = N = 16$ in static channel with $P = 8$ using symbol-DNN and MMSE detectors under t-distributed noise.

DNN architecture used for Fig. 3 and the parameters from Table II are used for Fig. 5. From Fig. 5, it can be seen that deviation from the Gaussian noise results in performance degradation of ML detector. This is because the ML decision rule in (12) is optimum only when noise is i.i.d. Gaussian and it is suboptimum for non-Gaussian noise. On the other hand, the symbol-DNN performs significantly better in non-Gaussian noise scenario. This is because of the inherent ability of the DNN to learn the underlying noise distribution. A similar performance behavior is observed in a larger OTFS system with $M = N = 16$, $P = 8$, and BPSK in Fig. 6. The DNN architecture used for Fig. 4 and the parameters from Table III are used for Fig. 6. It can be seen that the symbol-DNN detector performs very well while the performance of MMSE detector gets degraded in case of t-distributed noise.

C. BER in non-zero Doppler channel

Here, we consider the BER performance in non-zero Doppler channels, where the channel variations are slow in the DD domain. Figure 7 shows the BER performance of symbol-DNN and MMSE detectors under non-zero Doppler conditions. The system parameters considered are: $M = N = 16$,

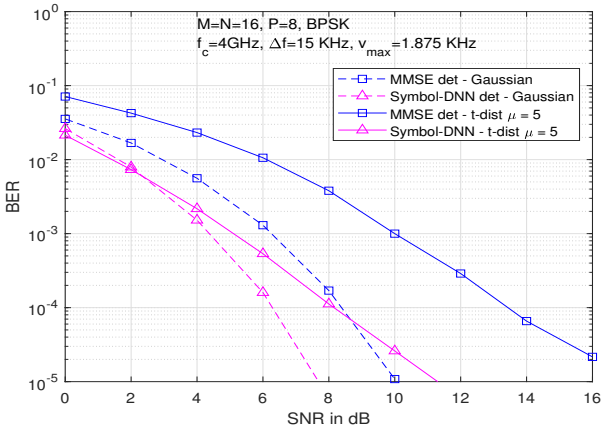

Fig. 7. BER performance of OTFS with $M = N = 16$ in non-zero Doppler channel with $P = 8$ under Gaussian and t-distributed noise.

Path, i	1	2	3	4	5	6	7	8
τ_i (μs)	0	4.16	8.32	12.48	16.64	20.8	24.96	29.12
ν_i (Hz)	0	0	938.5	938.5	938.5	1875	1875	1875

TABLE V
DELAY-DOPPLER PROFILE FOR FIG. 8.

$P = 8$, BPSK, $f_c = 4$ GHz, $\Delta f = 15$ KHz, and $\nu_{max} = 1.875$ KHz. The DD profile considered is given in the Table V. The DNN architecture of Fig. 4 and the parameters of Table III are considered for Fig. 7. The performance of symbol-DNN and MMSE detectors are compared for the cases of Gaussian noise and t-distributed noise. It can be observed that the symbol-DNN detector performs better than the MMSE detector in both the cases, where the performance advantage of symbol-DNN is more in the case of t-distributed noise.

D. BER in correlated noise in MIMO-OTFS

Here, we consider the BER performance of MIMO-OTFS in non-zero Doppler channel, where there is noise correlation across multiple receive antennas due insufficient spacing between them at the receiver. We consider a correlation model [19], where the noise correlation matrix is given by

$$\mathbf{N}_c = \begin{bmatrix} 1 & \rho & \rho^2 & \cdots & \rho^{n_r-1} \\ \rho & 1 & \rho & \cdots & \rho^{n_r-2} \\ & & & \ddots & \\ \rho^{n_r-1} & \rho^{n_r-2} & \cdots & & 1 \end{bmatrix}, \tag{13}$$

and ρ is the correlation coefficient such that $0 \leq \rho \leq 1$. The correlated noise across the receive antennas is $\mathbf{n}_c = \mathbf{N}_c\mathbf{n}$, where $\mathbf{n}$ is i.i.d. Gaussian noise. Figure 8 shows the BER performance of symbol-DNN and ML detectors when the noise is correlated across receive antennas with correlation coefficient $\rho = 0.4$. The performance of ML detector with i.i.d. Gaussian noise and modified ML detector for the case of correlated noise are also plotted for comparison. The decision rule for the modified ML detector is given by

$$\hat{\mathbf{x}} = \underset{\mathbf{x}\in\mathbb{A}^{MN}}{\arg\min}\ (\mathbf{y} - \mathbf{H}\mathbf{x})^H \Sigma^{-1} (\mathbf{y} - \mathbf{H}\mathbf{x}), \tag{14}$$

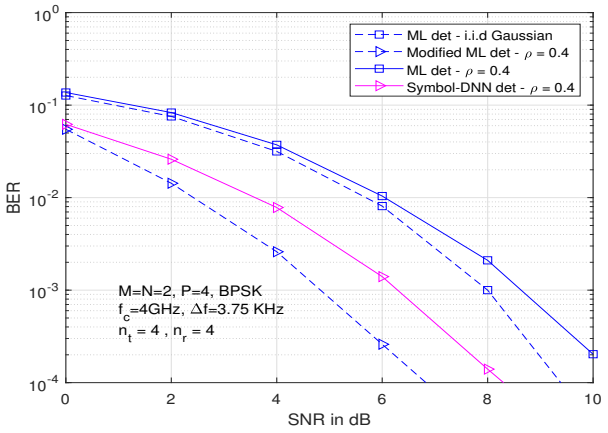

Fig. 8. BER performance of MIMO-OTFS system with $n_t = n_r = 4$, $M = N = 2$, $P = 4$, and BPSK in correlated noise using symbol-DNN and ML detectors.

where Σ is the estimated noise covariance matrix [20]. The system parameters considered are: number of transmit antennas $n_t = 4$, number of receive antennas $n_r = 4$, $M = N = 2, P = 4$, BPSK, $f_c = 4$ GHz, $\Delta f = 3.75$ KHz, and $\nu_{max} = 1.875$ KHz. The symbol-DNN architecture used for detection is as follows.
Symbol-DNN: input $\rightarrow$ 32 $\rightarrow$ ReLU $\rightarrow$ 8 $\rightarrow$ ReLU $\rightarrow$ 16 $\rightarrow$ ReLU $\rightarrow$ 2 $\rightarrow$ Softmax.
The DNN is trained for 100 epochs with 80000 training examples at a training SNR = 4 dB.

It can be observed from Fig. 8 that the symbol-DNN detector performs better than the conventional ML detector in (12) because i) the ML detection in (12) is suboptimum for correlated noise and ii) the DNN learns the underlying noise model including the noise correlation associated with the receive antennas. The modified ML detector in (14) gives the best performance as it is optimum for the correlated noise case. However, it has high computational complexity. On the other hand, the proposed symbol-DNN detector scales well for larger systems in the case of correlated noise.

V. Conclusion

We investigated a low-complexity symbol-DNN architecture for OTFS signal detection and demonstrated its efficiency in terms of both error performance and complexity. The considered DNN based detector could effectively learn the underlying noise models in practical scenarios where the noise deviates from the standard i.i.d. Gaussian model and outperform conventional ML and MMSE detectors. The DNN based detection approach for OTFS has good potential with promising directions for future work, which include convolutional neural networks that may require less number of trainable parameters.

References

[1] R. Hadani et al., "Orthogonal time frequency space modulation," in *Proc. IEEE WCNC'2017*, Mar. 2017, pp. 1-6.

[2] R. Hadani et al., "Orthogonal time frequency space modulation," Aug. 2018. [Online]. Available: https://arxiv.org/abs/1808.00519v1

[3] G. D. Surabhi, R. M. Augustine, and A. Chockalingam, "On the diversity of uncoded OTFS modulation in doubly-dispersive channels," *IEEE Trans. Wireless Commun.*, vol. 18, no. 6, pp. 3049-3063, Jun. 2019.

[4] S. K. Mohammed, "Derivation of OTFS modulation from first principles," Jul. 2020. [Online]. Available: https://arxiv.org/abs/2007.14357v1

[5] P. Raviteja, K. T. Phan, Y. Hong, and E. Viterbo, "Interference cancellation and iterative detection for orthogonal time frequency space modulation," *IEEE Trans. Wireless Commun.*, vol. 17, no. 10, pp. 6501-6515, Oct. 2018.

[6] K. R. Murali and A. Chockalingam, "On OTFS modulation for high-Doppler fading channels," in *Proc. ITA'2018*, Feb. 2018, pp. 1-10.

[7] R. Hadani and A. Monk, "OTFS: A new generation of modulation addressing the challenges of 5G," Feb. 2018. [Online]. Available: https://arxiv.org/abs/1802.02623

[8] P. Raviteja, E. Viterbo, and Y. Hong, "OTFS performance on static multipath channels," *IEEE Wireless Commun. Lett.*, vol. 8, no. 3, pp. 745-748, Jun. 2019.

[9] J. Zhang, A. D. S. Jayalath, and Y. Chen, "Asymmetric OFDM systems based on layered FFT structure," *IEEE Signal Proces. Lett.*, vol. 14, no. 11, pp. 812-815, Nov. 2007.

[10] S. Dorner, S. Cammerer, J. Hoydis, and S. t. Brink, "Deep learning based communication over the air," *IEEE J. Sel. Topics in Signal Process.*, vol. 12, no. 1, pp. 132-143, Feb. 2018.

[11] T. O'Shea and J. Hoydis, "An introduction to deep learning for the physical layer," *IEEE Trans. Cognitive Commun. and Netw.*, vol. 3, pp. 563-575, Dec. 2017.

[12] Y. Jiang, H. Kim, H. Asnani, S. Kannan, S. Oh, and P. Viswanath, "LEARN codes: inventing low-latency codes via recurrent neural networks," in *Proc. IEEE ICC'2019*, Jul. 2019.

[13] H. Kim, Y. Jiang, R. Rana, S. Kannan, and P. Viswanath, "Communication algorithms via deep learning," in *Proc. ICLR'2018*, Apr.-May 2018, pp. 1-17.

[14] N. Farsad and A. Goldsmith, "Neural network detection of data sequences in communication systems," *IEEE Trans. Signal Process.*, vol. 66, no. 21, pp. 5663-5678, Sep. 2018.

[15] N. T. Nguyen and K. Lee, "Deep learning-aided tabu search detection for large MIMO systems," *IEEE Trans. Wireless Commun.*, vol. 19, no. 6, pp. 4262-4275, Jun. 2020.

[16] B. Shamasundar and A. Chockalingam, "A DNN Architecture for the detection of generalized spatial modulation signals," *IEEE Commun. Lett.*, IEEE Xplore, doi: 10.1109/LCOMM.2020.3018260.

[17] T. V. Luong, Y. Ko, N. A. Vien, D. H. N. Nguyen, and M. Matthaiou, "Deep learning-based detector for OFDM-IM," *IEEE Wireless Commun. Lett.*, vol. 8, no. 4, pp. 1159-1162, Aug. 2019.

[18] T. Wu, "CNN and RNN-based deep learning methods for digital signal demodulation," in *Proc. ACM IVSP'2019*, Feb. 2019.

[19] S. Krusevac, P. Rapajic, and R. A. Kennedy, "Channel capacity estimation for MIMO systems with correlated noise," in *Proc. IEEE GLOBECOM'05*, Dec. 2005, pp. 2812-2816.

[20] M. L. Ammari and P. Fortier, "Analysis of MIMO receiver using generalized least squares method in colored environments," *J. Comput. Netw. and Commun.*, pp. 1-6, Aug. 2014.